All-dielectric apodized photonic crystals: A nondissipative pseudo-Hermitian system hosting multiple exceptional points

Abhishek Mondal [1], Shailja Sharma [1] and Ritwick Das [1,2,*]

[1] *School of Physical Sciences, National Institute of Science Education and Research, An OCC of Homi Bhabha National Institute, Jatni 752050, Odisha, India*

[2] *Optics and Photonics Center, Indian Institute of Technology Delhi, Hauz Khas, New Delhi 110016, India*

(Received 12 January 2023; accepted 21 April 2023; published 3 May 2023)

Optical systems obeying non-Hermitian dynamics have been the subject of intense and concerted investigation over the past two decades owing to their broad implications in photonics, acoustics, electronics, and atomic physics. A vast majority of such investigations rely on a dissipative, balanced loss-gain system which introduces unavoidable noise, and consequently this limits the coherent control of propagation dynamics. Here, we show that an all-dielectric, nondissipative photonic crystal (PC) could host at least two exceptional points in its eigenvalue spectrum. By introducing optimum apodization in the PC architecture, namely 1D-APC, we show that such a configuration supports a spectrum of exceptional points which distinctly demarcates the $\mathcal{PT}$-symmetric region from the region where $\mathcal{PT}$ symmetry is broken. The analytical framework allows us to estimate the geometric phase of the reflected beam and derive the constraint that governs the excitation of topologically protected optical Tamm-plasmon modes in 1D APCs.

DOI: 10.1103/PhysRevA.107.053502

I. INTRODUCTION

Optical systems which are governed by non-Hermitian Hamiltonian dynamics through an engineered gain and loss mechanism provide a route to overcome the limitations imposed by closed optical systems that obey the Hermitian-Hamiltonian-led dynamics. Such non-Hermitian systems give rise to a real eigenvalue spectrum when the Hamiltonian commutes with the parity-time ($\mathcal{PT}$) operator. A continuous change in the parameter governing the Hermiticity (of the Hamiltonian) breaks the $\mathcal{PT}$ symmetry which manifests in the form of a complex eigenvalue spectrum. In the parameter space, such points where the real and complex eigenvalues coalesce are termed as exceptional points (EPs) [1–3]. This spontaneous $\mathcal{PT}$-symmetry breaking has catalyzed a plethora of nonintuitive outcomes such as directional invisibility [4,5], coherent perfect lasing and absorption [6–11], negative refraction [12], single-particle based sensing [13–15], distortion-free wireless optical power transfer [16], and a few more [17–22]. It is, however, worth noting that the incommensurate gain and loss distribution in non-Hermitian systems impose the primary limitation on the practical applications due to unpredictable signal-to-noise ratio near EP [23–26]. In order to circumvent such bottlenecks, a few possibilities have been explored. One such promising route employs an asymmetric loss in the system (without gain) whose dynamics could be explored using a non-Hermitian Hamiltonian with a uniform background loss [23,27–29]. Such a configuration would exhibit $\mathcal{PT}$ symmetry that could be broken through scaling up the loss asymmetry. In a different scheme, a pseudo-Hermitian system was explored which allowed strong coupling between a large number of modes via manipulation of the parameters governing the Hamiltonian [27]. This led to the existence of EPs of multiple order and the interaction of eigenvalues around each EP provides a robust control on the propagation dynamics [30–32]. In spite of the aforementioned developments, a useful and practical proposition would be to devise a configuration hosting a multitude of EPs with the constraint that the electromagnetic (EM) energy lost due to the non-Hermitian dynamics is stored in a reservoir. This essentially implies that the dissipative channel associated with a non-Hermitian system drives a separate Hermitian system which could allow reverse flow of EM energy by virtue of cyclical dynamics. Such systems have been explored in the area of parametric frequency conversion processes where the EM energy lost in one of the parametric processes (obeying non-Hermitian dynamics) is coherently transferred to another parametric process that follows a Hermitian dynamics [33]. A plausible translation of such an idea in the nonabsorptive linear systems would be to introduce a *virtual* loss in an intermodal interaction process thereby generating multiple EPs in the parameter space. One of the simplest configurations imitating such a process is a multimodal interaction in an all-dielectric one-dimensional (1D) photonic-crystal (PC) with a gradually varying duty cycle (for each unit cell). In such an apodized 1D-PC, the forward (source) to backward (sink) mode-coupling dynamics is essentially governed by a pseudo-Hermitian Hamiltonian whose Hermiticity is determined by the apodization along the propagation direction. In the present work, we show the existence of multiple EPs in an apodized 1D-PC and develop an analytical framework for ascertaining the possibility of exciting topologically protected optical edge modes in such aperiodically stratified configurations.

*dasritwick@opc.iitd.ac.in

II. THEORETICAL FRAMEWORK AND COUPLED-MODE FORMALISM

We consider a 1D-PC comprised of periodic bilayers with refractive indices n_1 and n_2 with thicknesses d_1 and d_2. Such conventional 1D-PCs or alternatively, distributed Bragg reflectors (DBRs) are usually characterized by photonic bandgaps (PBGs) which are separated from each other by high transmission (or pass) bands. In order to appreciate the EM wave propagation dynamics, we consider the coupling between pth mode ($|p\rangle$) with qth mode ($|q\rangle$), which could be represented employing the coupled-amplitude equations given by [34]

$$\frac{dA_q}{dz} = -i\frac{\beta_q}{|\beta_q|}\sum_p\sum_m \tilde{\kappa}_{qp}^{(m)} A_p e^{-i(\beta_q-\beta_p-m\frac{2\pi}{\Lambda})z} \tag{1}$$

where β_p and β_q are the longitudinal (z) components of wave vector k_p and k_q respectively. $\tilde{\kappa}_{qp}^{(m)}$ defines the strength of coupling (or coupling coefficient) between the pth and qth mode that is coupled through the mth Fourier component of the periodic dielectric distribution ($\Lambda = d_1 + d_2$). The factor $\Delta\beta = \beta_q - \beta_p - m\frac{2\pi}{\Lambda}$ (known as the phase mismatch) is one of the dynamical variables (along with $\tilde{\kappa}_{qp}$) which govern the measure of optical power transferred from one mode to the other. For the present work, we consider a contra-directional coupling setup where a forward (along $+z$) propagating mode ($|p\rangle \equiv |f\rangle$) is coupled to a backward (along $-z$) propagating mode ($|q\rangle \equiv |b\rangle$). Accordingly, it could asserted that $\beta_b = -\beta_f$ or alternatively $\Delta\beta = 2\beta_f - \frac{2\pi}{\Lambda}$ and therefore, Eq. (1) could be simplified to [34]

$$\frac{dA_b}{dz} = i\tilde{\kappa}A_f e^{-i\Delta\beta z}, \tag{2}$$

$$\frac{dA_f}{dz} = -i\tilde{\kappa}^* A_b e^{i\Delta\beta z}, \tag{3}$$

where $\tilde{\kappa} = \frac{i(1-\cos 2\pi\zeta)}{2\lambda}\frac{({n_1}^2-{n_2}^2)}{\bar{n}} = i\kappa$ and ζ is the dielectric filling fraction of layer with refractive index n_1 in the unit cell, i.e., $\zeta = \frac{d_1}{\Lambda}$. The mean refractive index for an unit cell of thickness Λ is $\bar{n} = \sqrt{\frac{d_1{n_1}^2+d_2{n_2}^2}{\Lambda}}$ and λ is the wavelength of operation. By using a gauge transformation given by $A_f \rightarrow \tilde{A}_f e^{i/2[\Delta\beta_0 z - \int_0^z q(z')dz']}$ and $A_b \rightarrow \tilde{A}_b e^{-i/2[\Delta\beta_0 z - \int_0^z q(z')dz']}$, we obtain [35]

$$i\frac{d}{dz}\begin{pmatrix}\tilde{A}_b\\ \tilde{A}_f\end{pmatrix} = \begin{pmatrix}-\Delta k & -\tilde{\kappa}\\ \tilde{\kappa}^* & \Delta k\end{pmatrix}\begin{pmatrix}\tilde{A}_b\\ \tilde{A}_f\end{pmatrix}. \tag{4}$$

Equation (4) is analogous to time-dependent Schrödinger's equation with *time* coordinate being replaced by *space* coordinate (z). Here, Δk ($= \frac{\Delta\beta}{2}$) and $q(z) = 0$ remains constant (for a given frequency) across the 1D PC which has a fixed duty cycle. The autonomous Hamiltonian $\hat{H} = -\vec{\sigma}\cdot\vec{B}$ with $\vec{\sigma} \equiv [\sigma_x, \sigma_y, \sigma_z]$ are the Pauli's spin matrices and $\vec{B} \equiv [0, \kappa, \Delta k]$ (magnetic field analog) represents a pseudo-Hermitian evolution dynamics. Alternatively, it is apparent that $\hat{H}^\dagger = \sigma_z^{-1}\hat{H}\sigma_z$, which renders the Hamiltonian to be pseudo-Hermitian, and therefore it could host purely real eigenvalues as governed by the parameters. In order to appreciate this point, we note that the eigenvalues of $\hat{H}$ are given by $e_{1,2} = \pm\sqrt{\Delta k^2 - \kappa^2}$ whereas the eigenfunctions

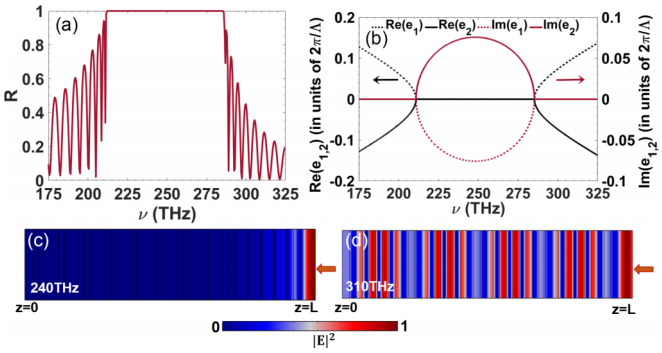

FIG. 1. (a) Reflection spectrum of a conventional (periodic) 1D PC. (b) Variation in Re(e_1) (dotted black curve), Im(e_1) (dotted maroon curve), Re(e_2) (solid black curve), and Im(e_2) (solid maroon curve) as a function of frequency (ν). [(c), (d)] Mode-field intensity for frequencies within the PBG 240 THz and that outside the PBG 310 THz respectively. The solid red arrow represents the direction of incidence of light.

corresponding to e_1 is expressed as $|\psi_1\rangle = (-i\frac{(\Delta k+\sqrt{\Delta k^2-\kappa^2})}{1^\kappa})$ and that for e_2 is $|\psi_2\rangle = (+i\frac{(-\Delta k+\sqrt{\Delta k^2-\kappa^2})}{1^\kappa})$. It is apparent that $\Delta k > \kappa$ (modes in the pass bands) have real eigenvalues and hence the forward-to-backscattered mode coupling is cyclic (with respect to z). On the other hand, $\Delta k < \kappa$ depicts a spectrum where the forward-to-backscattered mode coupling is unidirectional. In other words, the Hamiltonian $\hat{H}$ commutes with the parity-time ($\mathcal{PT}$) operator for $\Delta k > \kappa$ and therefore it is termed as $\mathcal{PT}$ symmetric with respect to forward-to-backscattered mode-coupling process. Here, the parity operator is defined as $\mathcal{P} \equiv \left(\begin{smallmatrix}0 & 1\\ 1 & 0\end{smallmatrix}\right)$ and $\mathcal{T}$ is an antilinear operator that performs the complex conjugation operation. For $\Delta k < \kappa$, the Hamiltonian $\hat{H}$ does not commute with $\mathcal{PT}$ operator and consequently the propagation characteristics pertain to $\mathcal{PT}$-symmetry broken phase. A closer look into the eigenvectors reveals that the equality $\kappa = \pm\Delta k$ manifests through coalescing of eigenvectors accompanied by vanishing eigenvalues. Such points in parameter space where κ equals $\pm\Delta k$ are termed as EPs and they distinctly demarcate the regions exhibiting Hermitian ($\mathcal{PT}$-symmetric phase) and non-Hermitian ($\mathcal{PT}$-symmetry broken phase) dynamical evolution of states (or modes).

In order to illustrate the aforementioned idea, we consider a practical 1D-PC with $n_1 \equiv$ TiO_2 layer and $n_2 \equiv$ SiO_2 layer. The layer thicknesses are $d_1 = d_2 = 150$ nm. The reflection spectrum for $N = 20$ unit cells is plotted in Fig. 1(a) which exhibits a high reflection band (or PBG) spreading over a 75 THz bandwidth. Here, R refers to the reflectivity from the 1D PC and ν ($= \frac{c}{\lambda}$) defines the frequency of the incident beam. In order to obtain the reflection spectrum, finite element method (FEM)–based simulations were carried out using the commercially available computational tool (COMSOL Multiphysics). In the simulations, the periodic boundary condition is imposed along the transverse direction and a mesh size of 5 nm is considered. We ignore the material dispersion for the simulations and assume $n_1 = 2.5$ ($\equiv TiO_2$) and $n_2 = 1.5$ ($\equiv SiO_2$) across the entire spectrum. For this 1D-PC, we also plotted the eigenvalues e_1 and e_2 [see Fig. 1(b)] as a function of frequency of the incident electromagnetic wave.

It is apparent that the eigenvalues vanish at $\nu_0 \approx 210$ THz and $\nu_0' \approx 285$ THz. These two frequencies (ν_0 and ν_0') define the EPs ($\kappa = +\Delta k$ and $\kappa = -\Delta k$) for the periodic 1D PC. A closer look would also reveal that the eigenvalues are purely imaginary within the PBG and at the band edges [see Fig. 1(a)] coincide with ν_0 and ν_0'. The mode-field spatial distribution for frequencies present within the PBG (240 THz) and outside the PBG (310 THz) are presented in Figs. 1(c) and 1(d) respectively. Figure 1(c) represents strong reflection from unit cells close to the entry face ($z = 0$) of the unit cell whereas Fig. 1(d) represents high delocalization of mode-field in the 1D-PC. In order to provide an analytical insight, we note that the extent of decay of mode-field for frequencies (ν) within the PBG is governed by the Bloch wave vector (K) [34]. The couple-mode formalism connects to the Bloch wave vector through the relation $K = \frac{2\pi}{\Lambda} + e_{1,2}$ which is complex within the PBG and purely real in the transmission bands [34,35]. In other words, Δk is much smaller than κ within the PBG and for $\nu = 240$ THz, $\Delta k \approx 0$. Therefore, predominantly κ determines the value of $e_{1,2}$ and in that case, the imaginary component of K maximizes. This essentially manifests through a rapid decay of mode field for $\nu = 240$ THz along z (propagation direction). It is worth noting that the investigations on systems exhibiting $\mathcal{PT}$ symmetry (or $\mathcal{PT}$ broken symmetry) led dynamics in photonics essentially involve optimally balanced gain-loss architectures such as segmented waveguides and photonic crystals. In such systems, a complex relative permittivity in different sections depicting *actual* gain or loss for the propagating light beam gives rise to the $\mathcal{PT}$ symmetry (or $\mathcal{PT}$ broken symmetry). The present configuration involving 1D PC does not include an *actual* dissipative component for achieving the $\mathcal{PT}$-symmetric to $\mathcal{PT}$-symmetry broken phase transition. Alternatively, the coupling of optical power to the backscattered mode $|b\rangle$ is analogous to a *virtual* loss for a forward propagating $|f\rangle$ mode. When this coupling is relatively weak i.e. $\Delta k > \tilde{\kappa}$, $|f\rangle$ and $|b\rangle$ exhibit cyclic exchange of optical power (as a function of z) which is an obvious outcome for a $\mathcal{PT}$-symmetric dynamics. On the other hand, a strong coupling regime where $\Delta k < \tilde{\kappa}$ manifests through a monotonic growth of modal power in the backscattered mode ($|b\rangle$). This is a distinct signature of $\mathcal{PT}$-symmetry broken phase. It is worthwhile to reiterate the point that the two regimes depicted by the inequality of Δk and $\tilde{\kappa}$ (in the parameter space) could be mapped onto the PBG and the transmission band(s) of the reflection spectrum. Subsequently, each PBG is necessarily bounded by two EPs in this framework. Additionally, these two EPs are fixed and cannot be tailored for a given 1D-PC with a fixed duty cycle and fixed period. Also, the conventional 1D-PC geometry excludes the possibility of realizing higher order exceptional points [36]. Taking a cue from this critical observation, we note that a small apodization or gradual change in dielectric filling fraction (ζ) of each unit cell of the 1D PC would allow us to realize discretely spaced (multiple) EPs at different optical frequencies (or wavelengths). In order to elucidate this point, we recall that Δk as well as $\tilde{\kappa}$ is a function of ζ. An optimum spatial variation in ζ could essentially give rise to the possibility of EPs at different physical locations (along z) in a 1D PC. As an example, we show below that an optimally apodized 1D PC

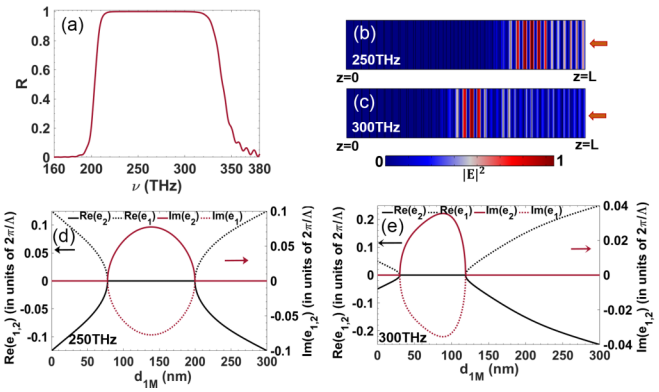

FIG. 2. (a) Reflection spectrum for designed 1D-APC. [(b), (c)] Mode-field intensities for two different frequencies, $\nu_a = 250$ THz and $\nu_b = 300$ THz, which are within the PBG of 1D-APC. [(d), (e)] Variation in Re(e_1) (dotted black curve), Im(e_1) (dotted maroon curve), Re(e_2) (solid black curve), and Re(e_2) (solid maroon curve) as a function of TiO_2 layer thickness for each unit cell (i.e., d_{1M}) at frequencies $\nu_a = 250$ THz and $\nu_b = 300$ THz respectively.

(1D APC) which satisfies the adiabatic constraints enables us to observe EPs at discreetly separated points along z.

A. Design of an 1D apodized PC and intermodal coupling

We consider a 1D APC configuration that exhibits varying dielectric filling fractions (ζ) in each unit cell. This variation is essentially dictated through the relation $d_{1M} = d_1 - M\delta$ and $d_{2M} = \Lambda - d_{1M}$. Here, d_{1M} and d_{2M} are the thickness of TiO_2 and SiO_2 layers respectively in the Mth unit cell ($M = 0, 1, 2, 3, ..., (N-1)$ for N number of unit cells). The unit cell period, however, remains unchanged i.e. $\Lambda = d_{1M} + d_{2M} = d_1 + d_2$. This apodization in 1D PC could be visualized through a longitudinal variation in Δk as well as $\tilde{\kappa}$ by virtue of a monotonic change in average refractive index ($\bar{n}$) for an *unit cell*. This variation in Δk and $\tilde{\kappa}$ in a 1D-APC geometry leads to an adiabatic evolution of modes along the propagation direction and manifests through a broader PBG (≈140 THz) in comparison with a conventional (periodic) 1D-PC [35]. This is presented in Fig. 2(a) which shows a broader reflection spectrum for the 1D-APC in comparison with the conventional 1D-PC [Fig. 1(a)]. In addition, a flat transmission band and the absence of sharp transmission resonances is a distinct feature of 1D APC reflection spectrum. The mode-propagation characteristics for the frequencies within the PBG (of 1D APC) is explored by drawing a comparison with the mode-field distributions for the equivalent modes within the PBG of a conventional 1D PC. Figures 2(b) and 2(c) shows the mode-field distribution for two frequencies $\nu_a = 250$ THz and $\nu_b = 300$ THz which are within the PBG of 1D APC. In comparison with the mode-field distribution shown in Fig. 1(c), it could be observed that different modes are reflected from spatially separated z values. The smaller frequency ($\nu_a = 250$ THz) is reflected from the regions which are closer to $z = 0$ edge of the 1D APC in comparison to that for $\nu_b = 300$ THz. From an analytical viewpoint, it is worthwhile to recall that the Bloch wave vector is expressed as $K = \frac{2\pi}{\Lambda} + e_{1,2}$. It is complex when $\Delta k < \kappa$

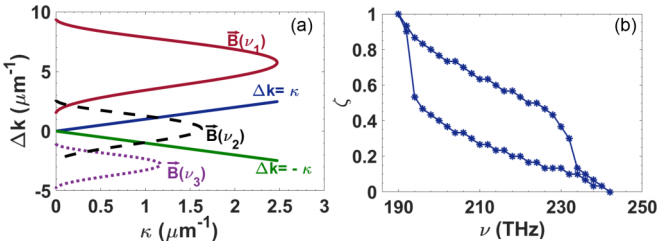

FIG. 3. (a) Variation of $\vec{B}$ in parameter space (spanned by κ and Δk) at different operating frequencies ($\nu_1 = 400$ THz, $\nu_2 = 250$ THz, $\nu_3 = 160$ THz) for the designed 1D APC. The blue and green solid lines represent the $\Delta k = \kappa$ and $\Delta k = -\kappa$ curves. (b) Location of EPs in different unit cells (with different filling fraction ζ) as a function of frequency (ν).

that happens for all the frequencies within the PBG for a conventional 1D PC. The imaginary component of K maximizes when $\Delta k = 0$ and accordingly, the mode-field decays sharply within one or two unit cells which could be seen in Fig. 1(c). Since, $\Delta k \equiv \Delta k(z)$ for 1D APC, Δk vanishes in different unit cells (d_{1M}) for different frequencies (ν). Therefore, in case of 1D-APC, the mode-field at different frequencies (within the PBG) strongly decays in different unit cells, which is apparent in Figs. 2(b) and 2(c).

From a different perspective, it is apparent that the variation in dielectric filling fraction (ζ) would result in different eigenvalues (and corresponding eigenvectors) for each unit cell. Accordingly, we plot the eigenvalues e_1 and e_2 as a function of d_{1M} for two frequencies $\nu_a = 250$ THz [Fig. 2(d)] and $\nu_b = 300$ THz [Fig. 2(e)] which are within the PBG of 1D APC. Each one of the figures show that the eigenvalues (e_1 and e_2) vanish at two different values of d_{1M} i.e. at the location of two different unit cells. Therefore, the 1D-APC geometry hosts two EPs for every d_{1M}. Consequently, for a multitude of ζ, there would be multiple EPs in the 1D APC for a forward-propagating mode to a backscattered mode-coupling process. As discussed before, the regions where Re(e_1) and Re(e_2) are nonzero in Figs. 2(d) and 2(e) exhibit a $\mathcal{PT}$-symmetric coupling dynamics between the forward-propagating and backscattered modes. On the other hand, in the regions where e_1 and e_2 are purely imaginary, the mode-coupling process exhibits $\mathcal{PT}$-symmetry-broken manifolds. The illustrations presented in Figs. 2(d) and 2(e) show that for each frequency within the PBG, the 1D APC hosts two EPs at two different d_{1M} (or ζ). This essentially implies that there exists one or more than one EPs hosted by each unit cell of the 1D APC. Therefore, an 1D APC is expected to host multiple EPs which are spectrally as well as spatially separated from each other. In order to ascertain the spectral location of EPs in the 1D APC, we plot the evolution of $\vec{B}$ in the parameter space for three different frequencies $\nu_1 = 400$ THz, $\nu_2 = 250$ THz, and $\nu_3 = 160$ THz, as shown in Fig. 3(a). It could be noted at ν_1 and ν_3 are situated outside PBG of 1D APC [see Fig. 2(a)]. Since the EPs are depicted by the condition $\Delta k = |\kappa|$, Fig. 3(a) also contains the curve $\Delta k = \pm\kappa$ (solid blue and green curves). It is apparent that $\Delta k = \pm\kappa$ curve intersects $\vec{B}_{\nu_2}$ at two points and it does not intersect the $\vec{B}_{\nu_1}$ curve as well as the $\vec{B}_{\nu_3}$ curve in the parameter space. For frequencies close to the band edge of 1D APC (say 200 THz or 350 THz), it could be ascertained that there exists only one EP in the eigenvalue spectrum. This is primarily due to the adiabatic constraints followed by the 1D-APC design. In other words, for the band-edge frequencies, the forward-propagating and backscattered modes are decoupled ($\tilde{\kappa} = 0$) at entry ($z = 0$) and exit ($z = L$) face of the crystal. Additionally, $d_{1M} = \Lambda$ for $m = 0$ (or $d_{2M} = \Lambda$ for $m = N$) in case of band-edge frequencies that leads to $\Delta k = 0$ for $\zeta = 1$. Therefore, $\tilde{\kappa} = \Delta k = 0$ depicts the *only* EP for the band-edge frequencies.

In order to elucidate the aforementioned point, we present the spectral location of EPs as a function of dielectric filling fraction (ζ) or propagation direction (z) in Fig. 3(b). It could be observed that there exist two EPs (at different ζ or z) for all the frequencies well within the PBG of 1D APC. However, for the band-edge frequencies ($\nu_l = 200$ THz and $\nu_h = 330$ THz), the 1D APC hosts one EP only. Nevertheless, the area enclosed by the EPs in Fig. 3(b) represents the region of $\mathcal{PT}$-symmetry-broken phase for the 1D APC. It is interesting to note that the separation between the two EPs for frequencies closer to the band edges (say $\nu \leqslant 210$ THz or $\nu \geqslant 310$ THz) is diminished and they tend to overlap at the same filling fraction. For appreciating this point, we note that such EPs are physically positioned *close to* the entry ($z = 0$) and exit ($z = L$) face of the 1D APC where $\tilde{\kappa}$ is very small [35]. By virtue of this, the PBG corresponding to those unit cells of 1D APC is relatively smaller in comparison with the PBG for a unit cell close to the center ($z \approx \frac{L}{2}$) of 1D APC. Due to the fact that the EPs exist at the band edges of PBG, a smaller PBG would essentially imply closely spaced EPs near the band edges [see Fig. 3(b)].

B. Geometric phase acquired by the backscattered modes

It is well known that the geometric phase of a pass band (or transmission band) for a one-dimensional conventional photonic crystal is quantized (0 or π) and it is known as the "Zak" phase. In this context, a geometric interpretation of backscattered (or reflection) phase from a 1D PC is trivial. In the case of 1D APC, the reflection of different spectral components (within the PBG) takes place from different unit cells (or z) along the propagation direction [35]. For example, the adiabatic following constraint leads to the conversion of optical power from the forward-propagating to the backscattered mode predominantly toward the exit face of 1D APC for frequency $\nu_2 = 250$ THz which could be seen in Fig. 4(a). Through a similar route, it could be shown that different spectral components within the PBG are reflected strongly from different unit cells of 1D APC [35]. For each spectral component (ν) in the PBG, the variation of $\tilde{\kappa}$ and Δk along z is nonidentical. Consequently, the estimation of geometric phase acquired by different backscattered modes is expected to be different and must play a crucial role in establishing the *bulk-boundary* correspondence in the case of 1D APC. In order to obtain the geometric phase (γ), we consider a triad defining the state vector $\vec{S}$ ($\equiv [u, v, w]$) where $u = \tilde{A}_i\tilde{A}_r^* + \tilde{A}_r\tilde{A}_i^*$, $v = -i[\tilde{A}_i\tilde{A}_r^* - \tilde{A}_r\tilde{A}_i^*]$ and $w = |\tilde{A}_r|^2 - |\tilde{A}_i|^2$ [35]. The z component of the state vector (w) represents the conversion efficiency of optical power from a forward-propagating mode to a backscattered mode [35]. Alternately, this is equivalent

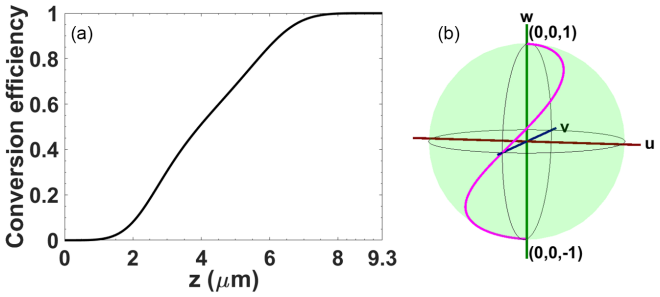

FIG. 4. (a) Variation in conversion efficiency ($\frac{w+1}{2}$) for optical power transfer between a forward-propagating mode to a backscattered mode as a function of 1D-APC length (z) for a frequency $\nu_2 = 250$ THz which is within the PBG. (b) State-vector ($\vec{S} = [u,\ v,\ w]$) trajectory on the Bloch sphere for $\nu_2 = 250$ THz.

to *reflectivity* from 1D APC. It is also worth noting that the trajectory of the state vector ($\vec{S}$) corresponding to the frequencies within the PBG ($\mathcal{PT}$-symmetry-broken region) is nonclosed. Consequently, the geometric phase is not a conserved quantity during the dynamical evolution of $\vec{S}$. In general, the solid angle subtended by the state-vector trajectory at the center of the Bloch sphere is used for computing the geometric phase. However, in the case of an adiabatic evolution, the state-vector trajectory could be very complicated. In Fig. 4(b), we have plotted such a state-vector trajectory (on the Bloch sphere) corresponding to a frequency $\nu = 250$ THz (which is within the PBG of 1D APC). It is important to note that $\vec{S} = [0, 0, -1]$ and $\vec{S} = [0, 0, 1]$ represent states in which all the optical power ($\propto |\tilde{A}_{f,b}|^2$) is present in the forward-propagating mode and backscattered mode respectively. Although the adiabatic evolution of state-vector results in complete optical power transfer from the forward to backward-propagating mode i.e. $w = -1$ to $w = 1$, the estimation of acquired geometric phase is unavoidably complicated owing to the spiralling trajectory of $\vec{S}$ on the Bloch-sphere. However, it is interesting to note that $\vec{S}$ goes from $[0, 0, -1]$ to [0,0,1] for all the frequencies (ν) within the PBG of 1D APC by virtue of satisfying the adiabatic following constraints. An important point is to note that the conversion efficiency (or reflectivity) is unity for all the frequencies within the PBG of 1D APC [35]. In other words, $\vec{B}$ goes from $[0, 0, -\Delta k]$ to $[0, 0, \Delta k]$ in the parameter space for all the PBG frequencies when the adiabatic following constraints are satisfied [35]. By virtue of the fact that the state vector $\vec{S}$ adiabatically follows $\vec{B}$ (as per the Bloch equation), the initial and the final values of $\vec{B}$ could also yield the geometric phase (γ). It is known that γ is estimated from angle ϕ (subtended by $\vec{B}$ at the origin $\Delta k = \tilde{\kappa} = 0$) through the relation $\gamma = \frac{\phi}{2}$. In that case, the geometric phase for each spectral component within the PBG is $\frac{\pi}{2}$. In order to elucidate this point, we plot $\vec{B}$ at different z (of 1D APC) in the parameter space for $\nu_2 = 250$ THz. This is shown in Fig. 5(a). At the entry face of 1D APC, $\vec{B}(z = 0) = [0, 0, -2.7\ \mu\text{m}^{-1}]$ (black arrow) and gradually goes to $\vec{B}(z = L) = [0, 0, +2.7\ \mu\text{m}^{-1}]$ (red arrow) at the exit face. At $z = \frac{L}{2}$, $\Delta k = 0$ and $\tilde{\kappa}$ is maximum [green arrow in Fig. 5(a)]. The evolution of $\vec{B}$ in Fig. 5(a) yields $\phi = \pi$ and consequently, $\gamma = \frac{\pi}{2}$. In a similar manner, γ for all the frequencies within the PBG would be $\frac{\pi}{2}$ by virtue of

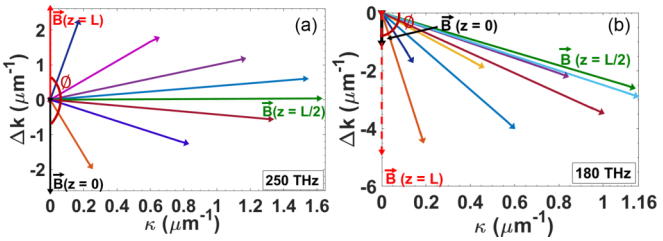

FIG. 5. Represents the evolution of $\vec{B}$ as a function of length (L) of 1D-APC in parameter ($\Delta k - \kappa$) space for (a) $\nu_2 = 250$ THz and (b) $\nu_4 = 180$ THz. ϕ represents the angle subtended by curve $\vec{B}$ at the origin.

adhering to the constraints imposed by adiabatic following. Hence, it could be asserted that a geometric phase of $\frac{\pi}{2}$ is acquired by a reflected beam in a 1D APC for the values of parameters which results in $\mathcal{PT}$-symmetry-broken phase. On the contrary, the variation in $\vec{B}$ is plotted as a function of z for $\nu = 180$ THz which is outside the PBG of 1D-APC [see Fig. 5(b)]. $\vec{B}(z = 0)$ (black arrow) and $\vec{B}(z = L)$ (red dashed arrow) are both negative as well as coparallel in this case. Consequently, the geometric phase $\gamma = \frac{\phi}{2} = 0$ for $\nu = 180$ THz. In addition, it is apparent that $\Delta k \neq 0$ at any point (or any z) in the 1D APC.

C. Tamm-plasmon excitations in 1D APC and the role of geometric phase

The presence of a plasmon-active layer adjacent to the all-dielectric 1D APC results in excitation of multiple Tamm-plasmon modes which are nondegenerate in the frequency spectrum. As an example, we consider a thin ($d_{Au} = 30$ nm) layer of gold placed in contact with high index layer (TiO_2) of 1D APC [see Fig. 6(a)]. The simulated reflection spectrum exhibits a sharp resonance within the PBG as shown in Fig. 6(b). These resonances are essentially due to Tamm-plasmon mode excitations which are highly localized electromagnetic states. Figure 6(b) depicts the existence of 10 Tamm-plasmon modes within the PBG of 1D APC. Although there are a few sharp resonances outside the PBG, their mode-field signatures do not resemble those for a Tamm-plasmon mode [37]. In general, the existence of Tamm-plasmon modes is governed by the condition $\phi_{\text{APC}} + \phi_{\text{Au}} = 2s\pi$ where $s = 0, 1, 2, 3, ...$ is a positive integer [38–40]. Here, ϕ_{APC} is the total phase acquired by the reflected beam from the 1D APC (light incident

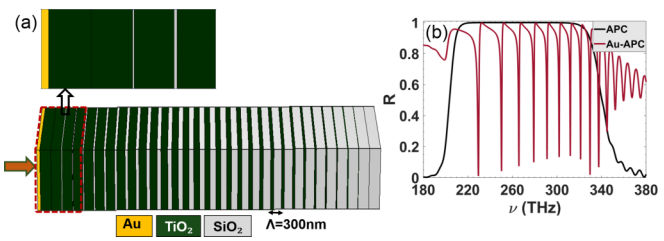

FIG. 6. (a) Schematic of the Au-1D-APC heterostructure. The Au layer is placed adjacent to the high-index TiO_2 layer. The thick brown arrow depicts the direction of light incidence on the Au-1D-APC. (b) Simulated reflection spectrum of 1D APC without Au (black solid curve) and that of Au-1D-APC (maroon solid curve).

from Au side), and ϕ_{Au} is the phase acquired by the reflected beam at the Au-TiO_2 interface. It is worthwhile to reiterate that the dielectric layer (of 1D APC) adjacent to the Au film is TiO_2 which is the high index layer. In the present context $\phi_{\mathrm{APC}} = \gamma + \alpha$, where α is the dynamic phase acquired by the reflected beam [35]. This could be estimated by noting the fact that the EPs (for a given frequency) are situated in different unit cells (or ζ) of the 1D APC. For a frequency ν, if the nearest EP (with respect to $z = 0$) is present in the Tth-unit cell of 1D APC, then α could be determined using

$$\alpha = \frac{2\pi\nu}{c}\sum_{M=0}^{T}[n_1 d_{1M} + n_2 d_{2M}]. \tag{5}$$

The knowledge of location for EPs in the 1D APC (obtained from the eigenvalue spectrum of $\hat{H}$) would accurately yield the dynamic phase (α) for any frequency of operation (ν). In conjunction with the estimate of γ, this information would allow us to determine the Tamm-plasmon mode resonance frequencies (ν_r). This recipe provides a flexibility in terms of designing an 1D APC which would facilitate excitation of Tamm-plasmon mode at a target (desirable) frequency (or wavelength) of operation. One such application could be the generation of higher harmonics or frequency downconversion using optical surface states [41]. In this case, the 1D APC could be designed such that the Tamm-plasmon modes (localized modes) have resonance frequencies that are governed by the energy conservation and phase-matching constraints associate with the frequency conversion process.

III. CONCLUSIONS

In conclusion, we presented an all-dielectric 1D-APC design which hosts multiple exceptional points in its eigenvalue spectrum by virtue of exhibiting a pseudo-Hermitian dynamics for a mode-coupling process between a forward-propagating mode to its backscattered counterpart. Although, the 1D-APC does not include any dissipative component, the intermodal coupling mechanism could be classified in terms of $\mathcal{PT}$-symmetric and $\mathcal{PT}$-symmetry-broken phases which are connected through a quantum phase transition. We also showed that the reflected beam (within the PBG) acquires a geometric phase of $\frac{\pi}{2}$ in the $\mathcal{PT}$-symmetry-broken phase. As a consequence of this outcome, the 1D APC could be designed for exciting the optical Tamm-plasmon modes at any desirable frequency within the PBG. This design flexibility allows us to employ such architectures for applications such as efficiently carrying out optical frequency conversion using surface states [41].

The data that support the findings of this study are available from the corresponding author upon reasonable request.

ACKNOWLEDGMENTS

The research is supported by the Science and Engineering Research Board, Government of India, Grant No. CRG/2020/000982. The authors would like to thank Dr. K. Saha (NISER) for the fruitful discussions and insightful comments.

The authors declare that there are no conflicts of interest related to this article.

[1] M. Berry, Physics of non-Hermitian degeneracies, Czech. J. Phys. **54**, 1039 (2004).
[2] W. D. Heiss, The physics of exceptional points, J. Phys. A: Math. Theor. **45**, 444016 (2012).
[3] E. J. Bergholtz, J. C. Budich, and F. K. Kunst, Exceptional topology of non-Hermitian systems, Rev. Mod. Phys. **93**, 015005 (2021).
[4] X.-F. Zhu, Y.-G. Peng, and D.-G. Zhao, Anisotropic reflection oscillation in periodic multilayer structures of parity-time symmetry, Opt. Express **22**, 18401 (2014).
[5] Z. Lin, H. Ramezani, T. Eichelkraut, T. Kottos, H. Cao, and D. N. Christodoulides, Unidirectional Invisibility Induced by $\mathcal{PT}$-Symmetric Periodic Structures, Phys. Rev. Lett. **106**, 213901 (2011).
[6] W. Wan, Y. Chong, L. Ge, H. Noh, A. Stone, and H. Cao, Time-reversed lasing and interferometric control of absorption, Science **331**, 889 (2011).
[7] Y. D. Chong, L. Ge, H. Cao, and A. D. Stone, Coherent Perfect Absorbers: Time-Reversed Lasers, Phys. Rev. Lett. **105**, 053901 (2010).
[8] S. Longhi, $\mathcal{PT}$-symmetric laser absorber, Phys. Rev. A **82**, 031801(R) (2010).
[9] S. Longhi, Non-Hermitian skin effect and self-acceleration, Phys. Rev. B **105**, 245143 (2022).
[10] Y. D. Chong, L. Ge, and A. D. Stone, $\mathcal{PT}$-Symmetry Breaking and Laser-Absorber Modes in Optical Scattering Systems, Phys. Rev. Lett. **106**, 093902 (2011).
[11] Y. Sun, W. Tan, H.-q. Li, J. Li, and H. Chen, Experimental Demonstration of a Coherent Perfect Absorber with PT Phase Transition, Phys. Rev. Lett. **112**, 143903 (2014).
[12] R. Fleury, D. L. Sounas, and A. Alù, Negative Refraction and Planar Focusing Based on Parity-Time Symmetric Metasurfaces, Phys. Rev. Lett. **113**, 023903 (2014).
[13] J. Wiersig, Sensors operating at exceptional points: General theory, Phys. Rev. A **93**, 033809 (2016).
[14] W. Chen, S. Ozdemir, G. Zhao, J. Wiersig, and L. Yang, Exceptional points enhance sensing in an optical microcavity, Nature (London) **548**, 192 (2017).
[15] J. Wiersig, Enhancing the Sensitivity of Frequency and Energy Splitting Detection by Using Exceptional Points: Application to Microcavity Sensors for Single-Particle Detection, Phys. Rev. Lett. **112**, 203901 (2014).
[16] H. Xu, D. Mason, L. Jiang, and J. Harris, Topological energy transfer in an optomechanical system with exceptional points, Nature (London) **537**, 80 (2016).
[17] L. Ge, Y. D. Chong, and A. D. Stone, Conservation relations and anisotropic transmission resonances in one-dimensional

$\mathcal{PT}$-symmetric photonic heterostructures, Phys. Rev. A **85**, 023802 (2012).

[18] J. Doppler, A. Mailybaev, J. Böhm, U. Kuhl, A. Girschik, F. Libisch, T. Milburn, P. Rabl, N. Moiseyev, and S. Rotter, Dynamically encircling exceptional points in a waveguide: Asymmetric mode switching from the breakdown of adiabaticity, Nature (London) **537**, 76 (2016).

[19] Y. Ota, R. Katsumi, K. Watanabe, S. Iwamoto, and Y. Arakawa, Topological photonic crystal nanocavity laser, Commun. Phys. **1**, 86 (2018).

[20] L. Ge and A. D. Stone, Parity-Time Symmetry Breaking beyond One Dimension: The Role of Degeneracy, Phys. Rev. X **4**, 031011 (2014).

[21] X. Zhu, H. Ramezani, C. Shi, J. Zhu, and X. Zhang, $\mathcal{PT}$-symmetric acoustics, Phys. Rev. X **4**, 031042 (2014).

[22] S. Longhi, Topological Phase Transition in Non-Hermitian Quasicrystals, Phys. Rev. Lett. **122**, 237601 (2019).

[23] K. Ding, Z. Q. Zhang, and C. T. Chan, Coalescence of exceptional points and phase diagrams for one-dimensional $\mathcal{PT}$-symmetric photonic crystals, Phys. Rev. B **92**, 235310 (2015).

[24] T. Goldzak, A. A. Mailybaev, and N. Moiseyev, Light Stops at Exceptional Points, Phys. Rev. Lett. **120**, 013901 (2018).

[25] J.-R. Li, L.-L. Zhang, W.-B. Cui, and W.-J. Gong, Topological properties in non-Hermitian tetratomic Su-Schrieffer-Heeger lattices, Phys. Rev. Res. **4**, 023009 (2022).

[26] F. Mostafavi, C. Yuce, O. S. Maganã Loaiza, H. Schomerus, and H. Ramezani, Robust localized zero-energy modes from locally embedded $\mathcal{PT}$-symmetric defects, Phys. Rev. Res. **2**, 032057(R) (2020).

[27] A. Guo, G. J. Salamo, D. Duchesne, R. Morandotti, M. Volatier-Ravat, V. Aimez, G. A. Siviloglou, and D. N. Christodoulides, Observation of $\mathcal{PT}$-Symmetry Breaking in Complex Optical Potentials, Phys. Rev. Lett. **103**, 093902 (2009).

[28] B. Peng, S. Ã–zdemir, S. Rotter, H. Yilmaz, M. Liertzer, F. Monifi, C. Bender, F. Nori, and L. Yang, Loss-induced suppression and revival of lasing, Science (New York, NY) **346**, 328 (2014).

[29] D. Leykam, K. Y. Bliokh, C. Huang, Y. D. Chong, and F. Nori, Edge Modes, Degeneracies, and Topological Numbers in Non-Hermitian Systems, Phys. Rev. Lett. **118**, 040401 (2017).

[30] C. Dembowski, H.-D. Gräf, H. L. Harney, A. Heine, W. D. Heiss, H. Rehfeld, and A. Richter, Experimental Observation of the Topological Structure of Exceptional Points, Phys. Rev. Lett. **86**, 787 (2001).

[31] S.-Y. Lee, J.-W. Ryu, S. W. Kim, and Y. Chung, Geometric phase around multiple exceptional points, Phys. Rev. A **85**, 064103 (2012).

[32] H. K. Gandhi, A. Laha, S. Dey, and S. Ghosh, Chirality breakdown in the presence of multiple exceptional points and specific mode excitation, Opt. Lett. **45**, 1439 (2020).

[33] N. Flemens and J. Moses, Hermitian Nonlinear Wave Mixing Controlled by a PT-Symmetric Phase Transition, Phys. Rev. Lett. **129**, 153901 (2022).

[34] A. Yariv and P. Yeh, *Optical Waves in Crystals Propagation and Control of Laser Radiation* (Wiley, New York, 1984).

[35] S. Sharma, A. Mondal, and R. Das, Geometric representation of adiabatic distributed-Bragg-reflectors and broadening the photonic band gap, Opt. Express **29**, 43303 (2021).

[36] A. Laha, D. Beniwal, S. Dey, A. Biswas, and S. Ghosh, Third-order exceptional point and successive switching among three states in an optical microcavity, Phys. Rev. A **101**, 063829 (2020).

[37] S. Sharma, A. Mondal, and R. Das, Infrared rainbow trapping via optical Tamm modes in an one-dimensional dielectric chirped photonic crystals, Opt. Lett. **46**, 4566 (2021).

[38] M. K. Shukla and R. Das, Tamm-plasmon polaritons in one-dimensional photonic quasi-crystals, Opt. Lett. **43**, 362 (2018).

[39] M. Xiao, Z. Q. Zhang, and C. T. Chan, Surface Impedance and Bulk Band Geometric Phases in One-Dimensional Systems, Phys. Rev. X **4**, 021017 (2014).

[40] A. P. Vinogradov, A. V. Dorofeenko, S. G. Erokhin, M. Inoue, A. A. Lisyansky, A. M. Merzlikin, and A. B. Granovsky, Surface state peculiarities in one-dimensional photonic crystal interfaces, Phys. Rev. B **74**, 045128 (2006).

[41] B. I. Afinogenov, A. A. Popkova, V. O. Bessonov, B. Lukyanchuk, and A. A. Fedyanin, Phase matching with Tamm plasmons for enhanced second- and third-harmonic generation, Phys. Rev. B **97**, 115438 (2018).